Final Draft
of the original manuscript:

Mohanty, D.; Paudel, P.; Gabrisch, H.:
Microstructure and magnetic behavior of compounds in the solid solution system Li [Ni1 − xMnx] O2 (x = 0.3, 0.5, 0.7)
In: Solid State Ionics (2010) Elsevier

DOI: 10.1016/j.ssi.2010.05.019

Microstructure and Magnetic Behavior of Compounds in the Solid Solution System Li [$Ni_{1-x}Mn_x$] O_2 (x=0.3, 0.5, 0.7)

D. Mohanty, P. Paudel, H. Gabrisch

Advanced Materials Research Institute, Department of Chemistry,

University of New Orleans, New Orleans, LA 70148, USA

Abstract

Layered Transition metal oxides containing more than one transition element are considered for applications in electric vehicles. In these compounds new and improved properties may result from the combination of element specific properties. At the same time the arrangement of species within the transition metal layer is one aspect that may affect the Li intercalation behavior and hence the electrochemical properties. Here we present a microstructural study on a series of Li [$Ni_{1-x}Mn_x$] O_2 compounds where the oxidations state and arrangement of TM ions are characterized by SQUID magnetometry and single crystal electron diffraction. Our results show that in plane long range ordering increases with Mn content and that Li/Ni interchange takes place in all powders but seems to be highest in Mn rich compositions. During chemical delithiation Li is removed from the TM layers leading to a decrease in percentage of long range ordering.

Key words: Magnetic susceptibility, Electron diffraction, Li-insertion compounds

Corresponding author: D. Mohanty, Advanced Materials research institute, University of New Orleans, 2000 Lake shore Drive, New Orleans, LA 70148,

e-mail dmohanty@uno.edu Tel. (504) 280 5569

1. Introduction

The need for Li-insertion compounds with high power and energy density motivates efforts to replace the layered Li-insertion compounds $LiCoO_2$ and $LiNiO_2$ with layered compounds of the solid solution system $LiCoO_2$- $LiNiO_2$- $LiMnO_2$. While $LiCoO_2$ is structurally instable when more than 0.5 Li is removed, $LiNiO_2$ with a high rechargeable capacity is difficult to synthesize reliably without interchange of Li and Ni between their respective layers [1-5]. The presence of Ni ions in the Li layers lowers the electrochemical activity of $LiNiO_2$ and its poor thermal stability in the charged state prohibits its practical usages [1, 6, 7]. Substituting manganese ions for Ni in the parent $LiNiO_2$ dramatically increases the thermal stability making $LiNi_{0.5}Mn_{0.5}O_2$ a promising, inexpensive alternate positive electrode material to $LiCoO_2$ and $LiNiO_2$ [8-10]. $LiNi_{0.5}Mn_{0.5}O_2$ is iso-structural to $LiNiO_2$, it has $R\bar{3}m$ symmetry as described by space group 166 , with Li in 3a sites, transition metal ions in 3b sites separated by cubic closed packed oxygen layers [11]. First principles calculations and x ray absorption experiments (XANES) of $LiNi_{0.5}Mn_{0.5}O_2$ showed that Ni and Mn are in the +2 and +4 state respectively in the as synthesized state [12]. During electrochemical cycling Ni is the active ion while Mn remains in the +4 state contributing towards the stability of this compound. However due to the very similar ionic radii of Ni^{+2} and Li^{+} ions there is always the possibility of interchanging nickel and lithium ions between their crystallographic sites. This exchange has been linked to the formation of long range in-plane ordering in form of $\sqrt{3}a_{hex}$ x $\sqrt{3}a_{hex}$ supercells in the TM layer [13-15]. A variation of the nickel to manganese ratio will change the oxidation state of nickel or manganese ions which may affect the electrochemical behavior [16]. XANES experiments confirmed the presence of Ni^{+3} in the nickel rich compound $LiNi_{1-x}Mn_xO_2$ ($0 \leq x \leq 0.5$) [16]. At the

same time different long range order schemes in the TM layer can be envisioned that do not require the exchange of Li and Ni ions between their respective layers. At Ni:Mn ratios 1:2 a honey comb like long range order is feasible resulting in super lattice reflections corresponding to the $\sqrt{3}a_{hex}$ x $\sqrt{3}a_{hex}$ supercells observed in $LiNi_{0.5}Mn_{0.5}O_2$ (assuming a sufficient difference between the atomic scattering factors of the two elements). This arrangement is observed in the TM layer of Li_2MnO_3 where a monoclinic unit cell is used to describe ordering between Li and Mn ions (C2/m symmetry, but ABAB stacking along c-axis as compared to ABC in $LiCoO_2$) [17].

Here the microstructure of $LiNi_{1-x}Mn_xO_2$ having Ni to Mn ratios of 1:2, 1:1 and 2:1 (x= 0.3, 0.5, 0.7) is characterized to monitor possible ordering mechanisms in the Ni rich and Mn rich compounds. We use single crystal electron diffraction to characterize long range ordering and magnetic measurements to investigate the oxidation states of transition metal ions as well as magnetic interactions between them. While magnetic data is available on Ni-rich compositions $LiNi_{1-x}Mn_xO_2$ ($0 \leq x \leq 0.5$) no information could be found on the Mn rich side of the binary phase diagram $LiNiO_2$-$LiMnO_2$ [16]. In first part we characterize the pristine material and in the second part lithium deficient phases are studied in order to understand the structural changes after lithium deintercalation.

2. Experimental

$LiNi_{1-x}Mn_xO_2$ (x= 0.3, 0.5, 0.7) was prepared following a co-precipitation method reported in literature [11]. Appropriate amounts of $NiNO_3.6H_2O$ and $MnNO_3.4H_2O$ were weighed according to the respective molar ratios and dissolved in water to obtain clear solutions of 2 molar concentrations. After stirring for 10-15 minutes 100 ml of 2 molar NaOH and 100 ml of 2 molar of NH_4OH were added and the mixtures were stirred under air for 24hr at a temperature T~ 40-50^{o}C. In the case of $LiNi_{0.3}Mn_{0.7}O_2$ the solutions were

stirred under Ar atmosphere. The precipitates were filtered, dried over night, and ground to obtain precursors. The required amount of $LiOH.H_2O$ was added, the mixture was ground and pre-sintered at 873^oC for 12 hrs, followed by annealing at 1173^oC in air for 12hrs. The as synthesized powders were chemically delithiated under Argon atmosphere at room temperature by using solutions of NO_2BF_4 in acetonitrile as delithiating agent. The reaction was carried out by drop wise addition of NO_2BF_4 solution over 90 minutes to $LiNi_{1-x}Mn_xO_2$ suspensions and allowing to react for additional 90 minutes under stirring. Quantitative analysis of Mn, Ni and Li content were carried through Inductive Coupled Plasma Mass Spectrometry (ICP-MS). The morphology of the obtained powders was observed by Scanning Electron Microscopy (SEM) using a JEOL JSM Scanning Electron Microscope. X-ray diffraction spectra (XRD) were collected with an X'pert PRO diffractometer (PAN analytical) operated at 40kV and 40mA current using Cu-K-α radiation. Silicon powder was used as internal diffraction standard. Phase determination was carried out by comparing experimental diffraction spectra to simulated powder diffraction spectra obtained with the software "Powder cell" and using unit cells published in literature [18]. Single crystal electron diffraction patterns were obtained using a JEOL 2010 Transmission Electron Microscope operated at 200kV. For comparison electron diffraction patterns were simulated using the software desktop microscopist. Magnetic measurements under field cooling (FC) and zero field cooling (ZFC) were performed using a superconducting quantum interface (SQUID) magnetometer (MPMS-XL-7: Quantum Design) in the temperature range between 5K and 300K under a magnetic field H=10kOe. Magnetic moment versus magnetic field (M-H) curves were obtained at 5K.

3. Results and discussions

3.1 Starting material

The compositions of the synthesized compounds obtained from ICP measurements are $Li_{1.02}Ni_{0.69}Mn_{0.29}O_2$, $Li_{0.99}Ni_{0.50}Mn_{0.52}O_2$ and $Li_{1.02}Ni_{0.30}Mn_{0.70}O_2$ confirming that the targeted Ni : Mn ratios have been realized. In Fig. 1 comparison of the particle morphologies illustrates that large octahedral particles (≈ 2μm) form in the Ni-rich material ($LiNi_{0.7}Mn_{0.3}O_2$) whereas smaller irregularly shaped particles are observed in $LiNi_{0.5}Mn_{0.5}O_2$ and $LiNi_{0.3}Mn_{0.7}O_2$.

The x-ray diffraction spectra of the synthesized powders are shown in Fig. 2a. All materials can be indexed in the α-$NaFeO_2$ structure and exhibit typical characteristics of a layered structure : clear splitting of (006)/(012) and (108)/(110) doublets and an intensity ratio I_{003} /I_{104} larger than one [3, 19]. The approximate c and a lattice parameter estimated from (003) and (110) peak positions take on the largest and smallest values in $LiNi_{0.5}Mn_{0.5}O_2$ and $LiNi_{0.3}Mn_{0.7}O_2$ respectively (c=14.33 Å, a=2.88 Å compared to c=14.28 Å, a=2.86 Å). The increase in lattice parameters with decreasing Ni-content observed between $LiNi_{0.7}Mn_{0.3}O_2$ and $LiNi_{0.5}Mn_{0.5}O_2$ is in agreement with observations published by Kobayashi et al [16]. In the Mn rich small additional diffraction peaks are observed in the 2-theta range of 20^o-35^o. In the Mn-rich compound these are in agreement with superstructure peaks resulting from in plane ordering in a $\sqrt{3}a_{hex}$ x $\sqrt{3}a_{hex}$ supercell that can be indexed either in a monoclinic unit cell (C2/m) or in a trigonal unit cell ($P3_112$) [17,20]. The positions of the superstructure peaks are marked by dots in Fig. 2a. The presence of super structure peaks was in agreement with the analysis of single crystal electron diffraction patterns where maximum long range ordering was observed for manganese rich phase presented below. Before discussing the single crystal diffraction

data the results of magnetic measurements are presented in order to assign the oxidation states of transition metal ions.

In Fig. 3 temperature dependence of the molar magnetic susceptibility is shown for experiments under field cooling (FC) and zero field cooling (ZFC). All the materials show paramagnetic behavior at high temperatures ($T \geq 150K$) and an increase in magnetic susceptibility in the lower temperature region. The FC and ZFC curves are identical for $LiNi_{0.5}Mn_{0.5}O_2$ and for the Mn rich compound. In the case of the nickel rich composition the FC and ZFC curves bifurcate at T=30K indicating the presence of magnetic frustration in the lattice which can be classified as spin glass like behavior or geometrical frustration [21]. Spin glass like behavior has been observed in $LiNiO_2$ has been linked to the presence of Ni^{+2} ions in the lithium layer [22].

We calculated the effective magnetic moment for each compound from a plot of inverse susceptibility versus temperature in the temperature region 150-300 K (see table 1). The experimental values were compared to theoretical values based on combinations of Ni^{3+}/Mn^{3+} (all three compounds) , $Ni^{2+}/Ni^{3+}/Mn^{4+}$ (Ni-rich) or $Ni^{2+}/Mn^{3+}/Mn^{4+}$ (Mn-rich) ions in high and low spin configurations. The best fit between experimental and theoretical effective magnetic moment for each composition is listed in table 1. It can be seen that $LiNi_{0.5}Mn_{0.5}O_2$, $LiNi_{0.7}Mn_{0.3}O_2$, and $LiNi_{0.3}Mn_{0.7}O_2$ are best represented as $LiNi_{0.5}{}^{+2}Mn_{0.5}{}^{+4}O_2$, $LiNi_{0.3}{}^{+2}Ni_{0.4}{}^{+3}Mn_{0.3}{}^{+4}O_2$ and $LiNi_{0.3}{}^{+2}Mn_{0.4}{}^{+3}Mn_{0.3}{}^{+4}O_2$ respectively. In the case of $LiNi_{0.5}Mn_{0.5}O_2$ and the Ni-rich compound $LiNi_{0.7}Mn_{0.3}O_2$ our results are in agreement with literature reports based on theoretical and EXAFS studies [15,16]. However no reports could be found for the Mn rich material. The experimental effective magnetic moment for Mn rich material is $3.06\mu_B$ which is close to the theoretical effective magnetic moment value resulting from 0.3 mol of Ni^{+2}, 0.3 mol of Mn^{+4} and 0.4

mol of Mn^{+3} (high spin). A model assuming 0.3 mol of Ni^{+3} (high spin) and 0.7 mol of Mn^{+3} (high spin) can be rejected as the x-ray diffraction and the electron diffraction analysis (below) reveal a high percentage of long range ordering involving among the Li ions and Ni^{+2} ions and/or Mn^{+4} ions.

Taking the assigned charges into account the magnetic frustration in the nickel rich material can be explained as follows. The nickel rich material contains Ni^{+2} and Ni^{+3} ions along with Mn^{+4} ions. The ionic radius of Ni^{+2} (0.69 Å) is very much similar to the Li^{+} ion (0.76 Å) opening a possibility of interchange between Ni^{+2} ions present in the transition metal (TM) layer and Li^{+} ion in lithium layer. Based on the Goodenough's theory the presence of Ni^{2+} ions in the lithium layer then introduces antiferromagnetic coupling with Ni^{3+} ions in the TM layer via 180^{o} exchange interaction along the Ni^{2+}-O-Ni^{3+} path as well as ferromagnetic coupling with Mn^{4+} ions in the TM layer via a 180^{o} Ni^{2+}-O-Mn^{4+} path [23]. These interactions create magnetic frustration between Ni^{+2}, $Ni^{+3,}$ and Mn^{4+} in the triangular lattice among these ions which is seen in magnetic susceptibility versus temperature curve (Fig 3a). The effect of competing ferro and anti ferromagnetic interactions can also be seen in the magnetization curves collected at 5K where hysteresis behavior is observed for $LiNi_{0.5}Mn_{0.5}O_2$ and for the Ni rich material, see Fig. 4. The hysteresis behavior for $LiNi_{0.5}Mn_{0.5}O_2$ is due to the strong 180^{o} Ni^{+2} (lithium layer)-O-Ni^{+2} (TM layer) ferromagnetic coupling present in this material as reported by several authors [16, 24]. In the case of Ni rich material the hysteresis is less pronounced than in $LiNi_{0.5}Mn_{0.5}O_2$ which indicates the presence of anti ferromagnetic interaction present in the lattice. In case of the Mn-rich compound ($LiNi_{0.3}Mn_{0.7}O_2$) purely paramagnetic behavior is observed without any hysteresis character.

Single crystal electron diffraction patterns were taken from 15 particles of each material and were classified into the following categories :

O3 : Diffraction patterns showing no superlattice reflections are assumed to represent random TM arrangement and are labeled O3 type patterns following the notation for LiCoO2 in a trigonal unit cell (space group 166), an example is shown in Fig. 5a. The reflections in these patterns are called fundamental reflections. When TM and Li ions are arranged in an ordered fashion within the oxygen framework additional (superlattice) reflections may appear.

Spinel : In a cubic spinel (space group 225) TM and Li ions occupy layers of interstitial sites in alternating ratios of 1:3 assigned to lattice sites 16d and 8a in superlattice reflections are observed halfway between fundamental reflections, an example is shown in Fig. 5b.

$\sqrt{3}a_{hex}$ x $\sqrt{3}a_{hex}$ $R30^{o}$ type of ordering and C2/m : Long range order within the TM layer can be observed when 2 or more species are present. In case of Li2MnO3 (Li[Li1/3Mn2/3]O2) a honey comb structure is formed that has been described in literature in a C2/m notation [25]. Here superlattice reflections divide the distance between fundamental reflections into three, corresponding to a threefold increase of the unit cell dimensions with respect to distances between oxygen atoms in the O3 structure. The large difference in atomic scattering factor between Li and Mn lends a strong intensity to the observed superlattice diffractions. Similarly superlattice reflections corresponding to a threefold increase of the in-plane unit cell can be observed when three species are ordered in a regular arrangement within the TM layer as described by Ohzuku et. al in a trigonal lattice ($P3_112$) [20]. Here the small difference in atomic scattering factor should result in lower intensity of the observed superlattice reflections. In the case of $LiNi_{0.5}Mn_{0.5}O_2$ the $\sqrt{3}a_{hex}$ x $\sqrt{3}a_{hex}$ $R30^{o}$ in plane ordering results from Li/Ni exchange

where the replacement of some Ni with Li in the TM layer introduces local variations of cations arrangement as described by Meng et. al. [13]. The two crystal structures used to describe the cations arrangement differ in the oxygen stacking that is cubic close packed in the trigonal model compared to hexagonal close packed (AB stacking) in the monoclinic structure. The oxygen lattice in the monoclinic structure is slightly distorted which is accounted for by the monoclinic angle. Only patterns that unambiguously fit into the monoclinic category are labeled C2/m. Examples for the monoclinic structure and $\sqrt{3}a_{hex}$ x $\sqrt{3}a_{hex}$ R30^{o} type ordering are shown in Fig. 6 a, b.

A summary of the analysis results is presented in table 2. Comparison shows that the Ni-rich system does not show in-plane ordering (14 out of 15 particles indexed as O3) whereas the highest percentage of in-plane ordering is observed in the Mn rich compound (10 out of 15 particles). Small amounts of spinel phase and O3 type diffraction patterns are found in $LiNi_{0.5}Mn_{0.5}O_2$ and in the Mn-rich compound, and in $LiNi_{0.5}Mn_{0.5}O_2$ a small amount of the monoclinic phase was observed.

The absence of long range order in the Ni-rich system is in contrast to the exchange of Ni^{+2} and Li^{+} ions between their respective layers. We conclude that the extent of Ni^{+2} / Li^{+} exchange is minor and the number of Li-ions in the TM layer is insufficient to create a $\sqrt{3}a_{hex}$ x $\sqrt{3}a_{hex}$ R30^{o} type long range in-plane ordering. This argument is supported by results published by Kobayashi et al. who studied the Ni-rich side of the series $LiNi_{1-x}Mn_xO_2$ (x= 0.1-0.5). The authors confirmed that the least Ni/Li exchange is observed in nickel rich material and that the amount of exchange increases with manganese ion content [16]. In $LiNi_{0.5}Mn_{0.5}O_2$ the interchange between Ni^{+2} in the TM layer and Li^{+} in the lithium layer creates the ordering between (Li^{+}, Ni^{+2}) and Mn^{+4} in the TM layer which generates the $\sqrt{3}a_{hex}$ x $\sqrt{3}a_{hex}$ R30^{o} superstructure as previously reported by other authors[13]. In the Mn-rich compound long range in-plane ordering may be the result of a

honey comb arrangement formed of Ni and Mn ions comparable to the ordering observed in Li_2MnO_3. Alternatively it may involve Li/Ni interchange as described above for $LiNi_{0.5}Mn_{0.5}O_2$. Assuming that superlattice reflections of sufficient intensity require the presence of Li in the TM layer it follows that the Li/Ni interchange is the highest in the Mn rich material where the largest percentage of in plane ordering is observed. This follows the trend mentioned above for a decrease in Li/Ni interchange in Ni-rich $LiNi_{1-x}Mn_xO_2$ (x= 0.1-0.5) [16] . A possible explanation for this behavior can be found from a comparison between electron densities around Ni^{3+} in Ni-rich compounds and Mn^{3+} in Mn compounds. The electron density of Mn^{+3} ions is higher than that of Ni^{+3} ions, resulting in higher repulsion between Mn^{+3} and Ni^{+2} ions in the TM layer of manganese rich material. This may be the driving force for the higher Ni^{+2} / Li^{+} (lithium layer) exchange which introduces the $\sqrt{3}a_{hex}$ x $\sqrt{3}a_{hex}$ $R30^o$ in-plane ordering in $LiNi_{0.3}Mn_{0.7}O_2$ observed here. The assumption that Li/Ni exchange plays a role in long range ordering observed in the manganese rich composition is confirmed by the high intensity of superlattice reflections observed in $LiNi_{0.3}Mn_{0.7}O_2$ compared to those observed in $LiNi_{0.5}Mn_{0.5}O_2$ (compare Fig. 7a to Fig 7b.).

3.2 Delithiated materials:

During chemical delithiation about 0.12 - 0.14 Li was extracted from the synthesized powders and the resulting compositions measured by ICP are $Li_{0.88}Ni_{0.68}Mn_{0.29}O_2$, $Li_{0.86}Ni_{0.48}Mn_{0.53}O_2$, and $Li_{0.87}Ni_{0.31}Mn_{0.65}O_2$. The corresponding x-ray diffraction patterns in figure 2 (b) show the following trends : The intensities of superlattice peaks for delithiated Mn rich material are lower than those observed in the Mn rich starting material , indicating that lithium ions have been extracted from the transition metal layers thereby reducing in long range ordering. In the Ni rich material the splitting between (110) and (018) doublet has decreased and the (006) peaks has disappeared,

corresponding to formation of some spinel phase. No major change was observed in the x-ray diffraction spectrum $Li_{0.88}Ni_{0.5}Mn_{0.5}O_2$.

A summary of the analysis of electron diffraction pattern taken from 15 particles of the delithiated compounds is given in table 3. A comparison to the relative amounts observed in the starting material shows that the percentage of in-plane ordering has decreased in the Mn-rich compound and in $Li_{0.87}Ni_{0.5}Mn_{0.5}O_2$. Furthermore the intensity of superlattice diffractions in the Mn-rich compound is weak compared to the intensity observed in the starting material. This indicates that less lithium is present in the transition metal layers compared to the starting material and that during chemical delithiation lithium is extracted from the TM layers. In the Ni-rich material an increase in ordering is observed in the form of spinel formation and formation of a monoclinic phase.

The magnetic behavior of the delithiated powders shows similar trends as the starting material, with the exception of the Ni-rich compound. Here the magnetic frustration behavior observed in the starting material has vanished after Li-extraction. In Figure 3(b) the variation of molar magnetic susceptibility values with the temperature is shown for field cooling (FC) and zero field cooling (ZFC) mode. The FC and ZFC curves are similar for all the materials showing paramagnetic behavior in the high temperature region ($T \geq 150K$) and increased magnetic susceptibility at lower temperature. The effective magnetic moments calculated from the plot of inverse susceptibility over temperature are lower than those measured in starting material, see table 1. To decide which ion compensates the charge upon Li-extraction in each compound we calculated the theoretical effective magnetic moment considzering oxidation of Ni^{2+}, Ni^{3+} or Mn^{3+}. The removal of 0.12 Li from $LiNi^{2+}_{0.5}Mn^{4+}_{0.5}O_2$ requires either oxidization of (i) 0.12mol of Ni^{+2} to Ni^{+3} (HS/LS) or (ii) 0.06 mol Ni^{+2} are oxidized to Ni^{+4} (HS/LS). The resulting compositions are (i) $Li^{+}_{0.88}Ni^{2+}_{0.38}Ni^{3+}_{0.12}Mn^{4+}_{0.5}O_2$ and (ii)

$Li^{+}_{0.88}Ni^{2+}_{0.44}Ni^{4+}_{0.06}Mn^{4+}_{0.5}O_2$. A comparison between the experimentally determined effective magnetic moment ($3.05\mu_B$) to the values determined for the two models shows that Ni^{+2} is oxidized to Ni^{+4} upon Li extraction from. Model (i) yields a theoretical effective magnetic moment of $3.22\mu_B$ compared to 3.08 μ_B for model (ii). Similar considerations for the Ni-rich and the Mn rich compounds do not yield unambiguous results. In the Ni-rich material an experimental effective magnetic moment of $2.50\mu_B$ is measured. This compares to a best theoretical value of $2.55\mu_B$ for oxidation of Ni^{2+} to Ni^{3+}(LS) or of $2.46\mu_B$ for oxidation of Ni^{3+} to Ni^{4+}. The oxidation of Ni^{2+} to Ni^{4+} can be excluded based on the larger discrepancies between theoretical and experimental values (closest fit : $2.55\mu_B$ and $2.50\mu_B$). For comparison in the Mn rich material the oxidation of Ni^{2+} to Ni^{3+} or to Ni^{4+} yields similar theoretical effective magnetic moments. $3.00\mu_B$ and $2.96\mu_B$ are calculated for Ni^{2+} (LS) $\rightarrow$ Ni^{3+} (LS) for Ni^{2+} (LS) $\rightarrow$ Ni^{4+} (LS) respectively compared to an experimental value of 3.03 μ_B. Here the oxidation of Mn^{3+} can be excluded.

4. Conclusions

Compounds in the series $LiNi_{1-x}Mn_xO_2$ (x= 0.3, 0.5, 0.7) were synthesized in the layered structure and characterized by powder and single crystal diffraction methods as well as magnetic measurements with super structure peaks were observed in the manganese rich phase . Comparison between theoretical models and experimentally determined effective magnetic moment indicates that Ni and Mn ions take on +2 and +4 oxidation states when present in a 1 : 1 ratio. In Ni rich or Mn rich compounds the extra Ni or Mn ions are observed in +3 oxidation states. Upon Li-extraction Ni^{2+} is oxidized to Ni^{4+} in $LiNi_{0.5}Mn_{0.5}O_2$. In all as synthesized materials exchange between Li^{+} and Ni^{+2} is observed that results in in-plane $\sqrt{3}a_{hex}$ x $\sqrt{3}a_{hex}$ $R30^o$ long range order in $LiNi_{0.5}Mn_{0.5}O_2$ and in the Mn-rich compound but not in the Ni-rich compound. However the observed

magnetic frustration in $LiNi_{0.7}Mn_{0.3}O_2$ indicates that Ni^{2+} ions are present in the Li layer here as well. After Li-extraction the magnetic frustration disappeared in the Ni-rich phase while the percentage of long range order decreased in $LiNi_{0.5}Mn_{0.5}O_2$ and in the Mn-rich phase indicating that Li has been extracted predominantly from the TM layer.

Acknowledgement

This work was supported through the Louisiana board of regents, Grant No. LEQSF(2007012)-ENH-PKSFI-PRS-04.

References

[1] O. J. Besenhard, "Handbook of Battery Materials." Wiley-VCH, New York, 1999.

[2] J. M. Paulsen, C. L. Thomas, and J. R. Dahn, Journal of Electrochemical Society **146**, 3560 (1999).

[3] J. R. Dahn, U. v. Sacken, and M. C.A., Solid State Ionics **44**, 87 (1990).

[4] R. Kanno, H. Kubo, Y. Kawamoto, T. Kamiyama, F. Izumi, T. Y., and M. Takano, Journal of Solid State Chemistry **11**, 216 (1994).

[5] H. Arai, S. Okada, H. Ohtsuka, M. Ichimura, and J. Yamaki, Solid State Ionics **8**, 261 (1995).

[6] A. Hirano, R. Kanno, Y. Kawamoto, T. Y., K. Yamaura, M. Takano, K. Ohyama, M. Ohashi, and Y. Yamaguchi, Solid State Ionics **78**, 123 (1995).

[7] L. Coguennec, C. Pouillerie, A. N. Masour, and C. Delmas, Journal of Materials Chemistry **11**, 131 (2001).

[8] N. Yabuuchi, Y. T. Kim, H. H. Li, and Y. Shao-Horn, Chemistry of Materials **20**, 4936 (2008).

[9] T. Ohzuku and Y. Makimura, Chemistry Letters **8**, 744 (2001).

[10] Z. Lu, D. D. Macneil, and J. R. Dahn, Electrochemical and Solid-State Letters **4**, A191 (2001).

[11] Y. Arachi, H. Kobayashi, S. Emura, Y. Nakata, M. Tanaka, and T. Asai, Chemistry Letters **32**, 60 (2003).

[12] J. Reed and G. Ceder, Electrochemical and Solid-State Letters **5**, A145 (2002).

[13] Y. S. Meng, G. Ceder, C. P. Grey, W.-S. Yoon, and Y. Shao-Horn, Electrochemical and Solid-State Letters **7**, A155 (2004).

[14] Y. S. Meng, G. Ceder, C. P. Grey, W.-S. Yoon, M. Jiang, J. Breger, and Y. Shao-Horn, Chemistry of Materials **17**, 2386 (2005).

[15] Y. Koyama, Y. Makimura, I. Tanaka, H. Adachi, and T. Ohzuku, Journal of Electrochemical Society **151**, A1499 (2004).

[16] H. Kobayashi, H. Sakaebe, H. Kageyeyama, K. Tatsumi, Y. Arachi, and T. Kamiyama, Journal of Materials Chemistry **13**, 590 (2003).

[17] J. Breger, M. Jiang, N. Dupre, Y. S. meng, Y. Shao-Horn, G. Ceder, and C. P. Grey, Journal of Solid State Chemistry **178**, 2575 (2005).

[18] H. Gabrisch, T. Yi, and R. Yazami, Electrochemical and Solid-State Letters **11**, A119 (2008).

[19] J. Morales, C. Perez-vicenet, and J. L. Tirado, Materials Research bulletin **623** (1990).

[20] Y. Koyama, N. Yabuuchi, I. Tanaka, H. Adachi, and T. Ohzuku, Journal of Electrochemical society **151**, A1545 (2004).

[21] S. Nagata, P. H. Keesom, and H. R. Harrison, Physical Review B **19**, 1633 (1979).

[22] A. Rougier, C. Delmas, and G. Chouteau, Journal of Physics and Chemistry of Solids **57**, 1101 (1996).

[23] J. B. Goodenough, Physical Review **117**, 1442 (1960).

[24] N. A. Chernova, M. MA, J. Xiao, M. S. Whittingham, J. Breger, and C. P. Grey, Chemistry of Materials **19**, 4682 (2007).

[25] C. H. Lei, J. G. Wen, M. Sardela, J. Bareno, I. Petrov, S.-H. Kang, and D. P. Abraham, Journal of Materials Science **44**, 5579 (2009).

Figure captions

Fig 1: Figure 1. Scanning electron micrographs of $LiNi_{1-x}Mn_xO_2$: (a.) x=0.3 (b), x = 0.5, (c) x = 0.7.

Fig 2: X-ray diffraction pattern of $LiNi_{1-x}Mn_xO_2$ (x=0.3, 0.5, 0.7) before chemical delithiation (a) and after chemical delithiation (b).

Fig 3: Variation of molar magnetic susceptibility versus temperature for $LiNi_{1-x}Mn_xO_2$ before chemical delithiation (a) and after chemical delithiation (b).

Fig 4: Magnetic moment (M) and Field (H) plots of $LiNi_{1-x}Mn_xO_2$.

Fig 5: Example of electron diffraction pattern showing O3 (a) and spinel reflections (b).

Fig 6: Example of electron diffraction pattern showing monoclinic (a) and $\sqrt{3}a_{hex}$ x $\sqrt{3}a_{hex}$ $R30^o$ type ordering reflections (b).

Fig 7: Example of electron diffraction pattern of starting material of $LiNi_{0.5}Mn_{0.5}O_2$ (a) and $LiNi_{0.3}Mn_{0.7}O_2$ (b) showing reflections having $\sqrt{3}a_{hex}$ x $\sqrt{3}a_{hex}$ type of ordering.

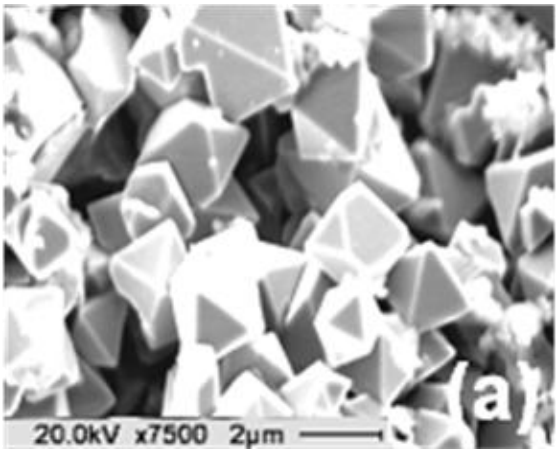

Fig 1(a)

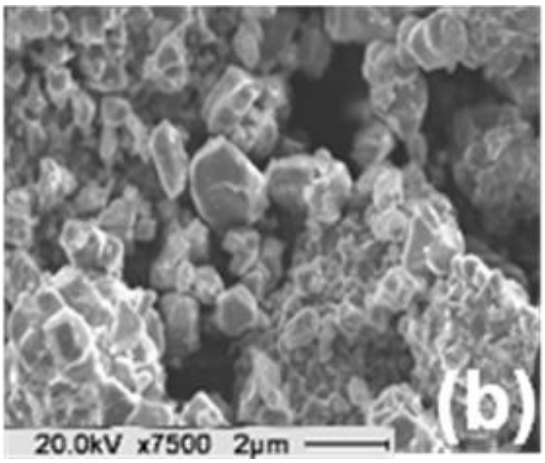

Fig 1(b)

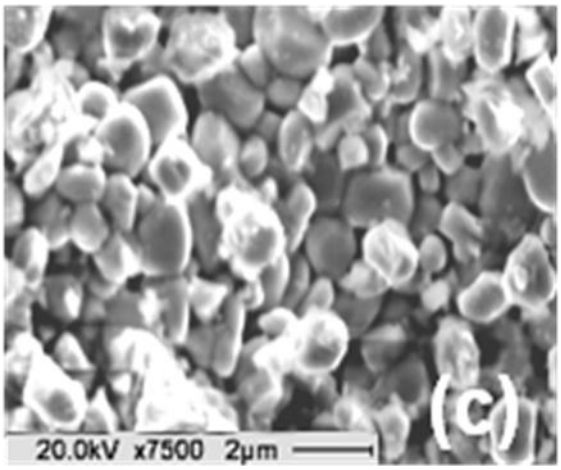

Fig 1(c)

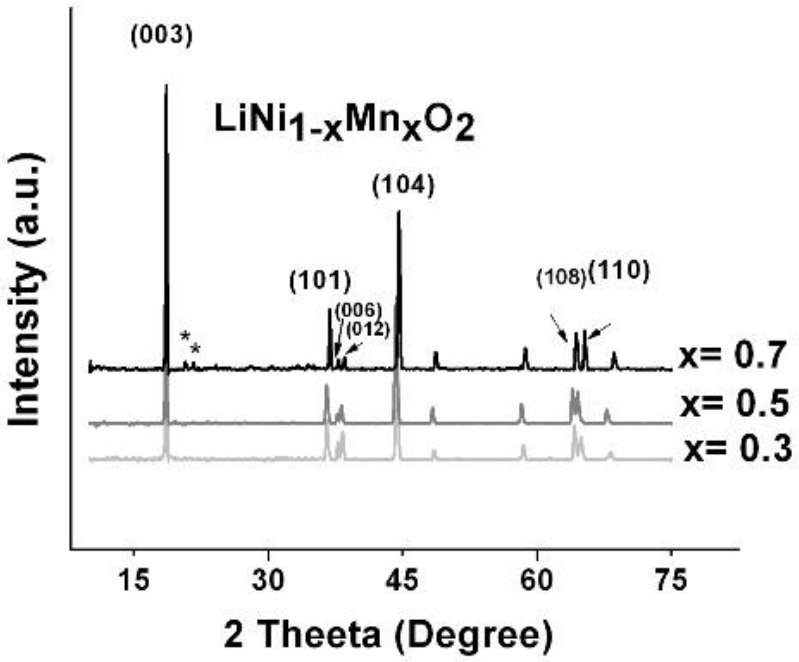
(003)
LiNi1-xMnxO2
(104)
(101)
(006)
(012)
(108)
(110)
x= 0.7
x= 0.5
x= 0.3
Intensity (a.u.)
15
30
45
60
75
2 Theeta (Degree)

Fig2(a)

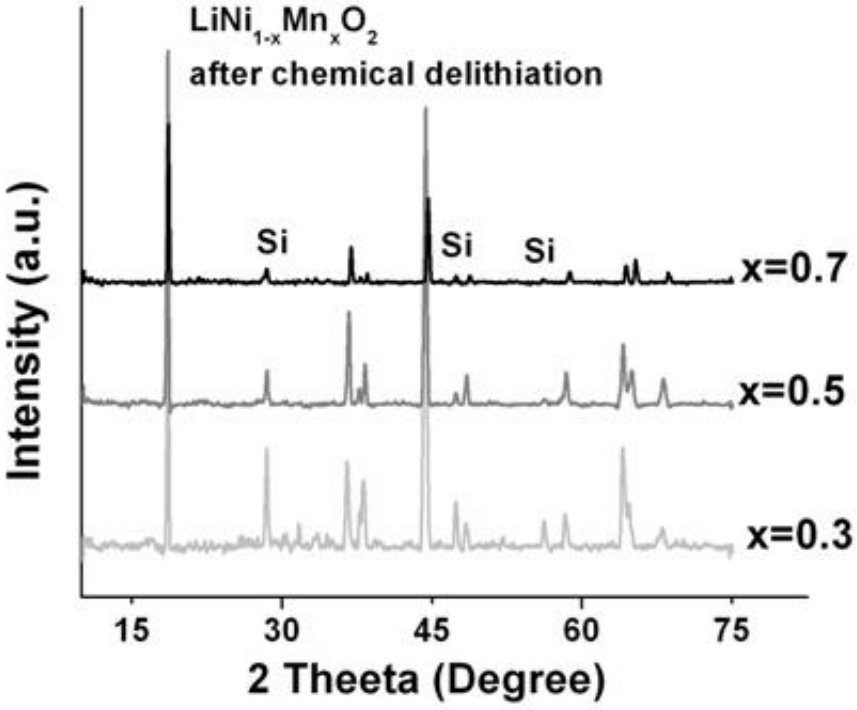
LiNi1-xMnxO2
after chemical delithiation
Si
Si
Si
x=0.7
x=0.5
x=0.3
Intensity (a.u.)
15
30
45
60
75
2 Theeta (Degree)

Fig 2 (b)

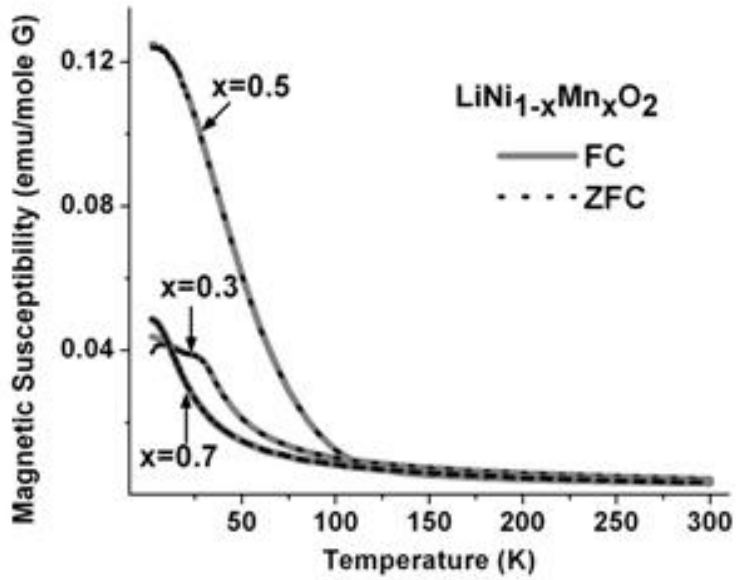
Magnetic Susceptibility (emu/mole G)
0.12
0.08
0.04
x=0.5
x=0.3
x=0.7
LiNi1-xMnxO2
FC
ZFC
50
100
150
200
250
300
Temperature (K)

Fig 3 (a)

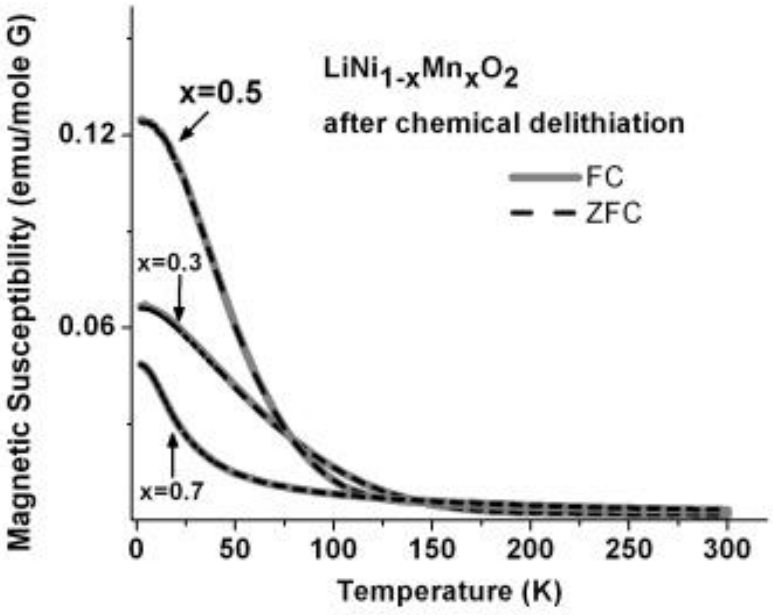
Magnetic Susceptibility (emu/mole G)
0.12
0.06
x=0.5
x=0.3
x=0.7
LiNi1-xMnxO2
after chemical delithiation
FC
ZFC
0
50
100
150
200
250
300
Temperature (K)

Fig 3 (b)

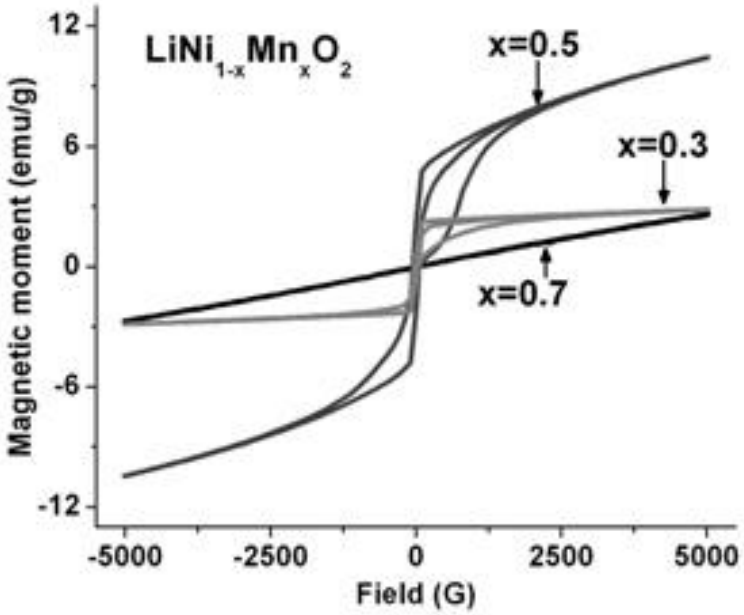
LiNi1-xMnxO2
x=0.5
x=0.3
x=0.7
Magnetic moment (emu/g)
12
6
0
-6
-12
-5000
-2500
0
2500
5000
Field (G)

Fig 4

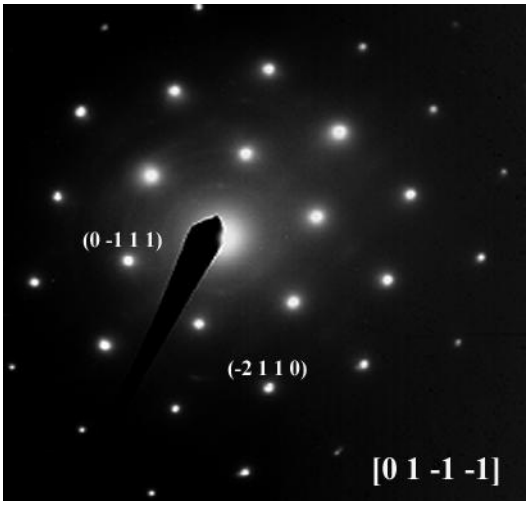

Fig 5 (a)

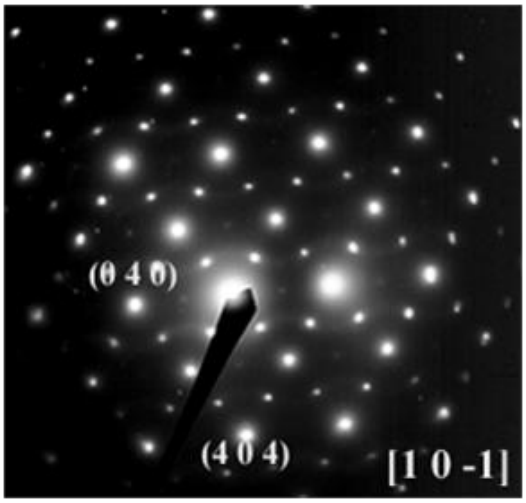

Fig 5 (b)

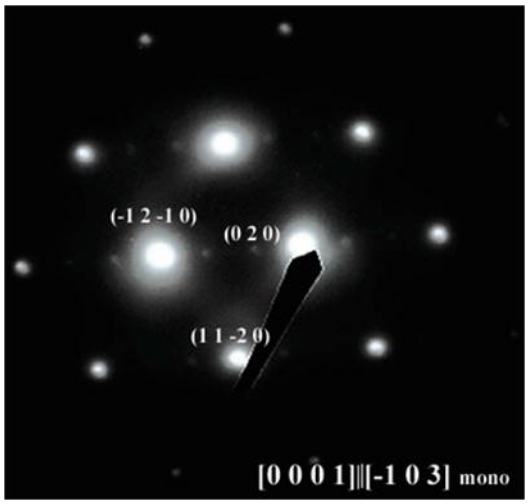

Fig 6 (a)

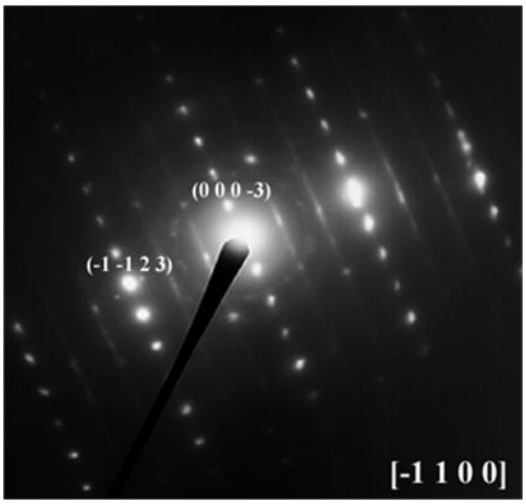

Fig 6 (b)

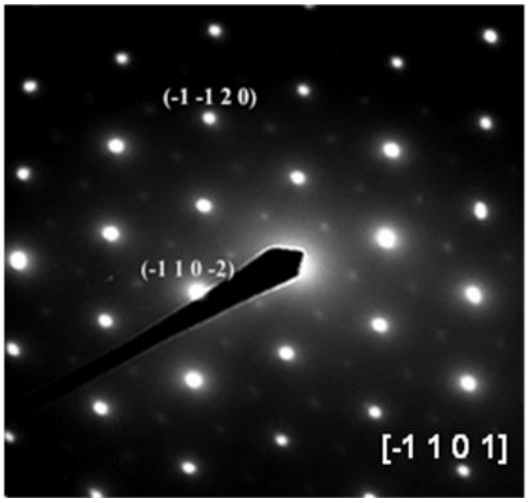

Fig 7 (a)

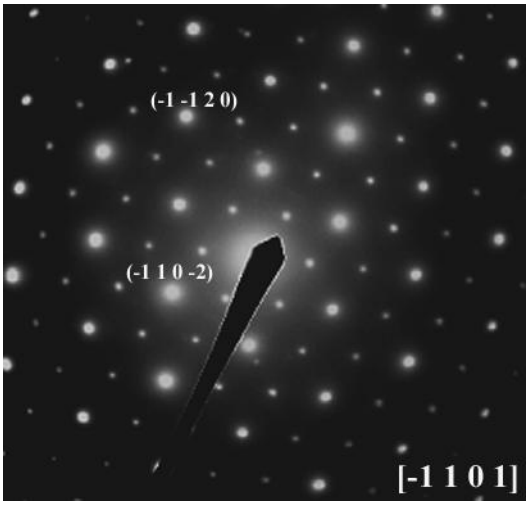

Fig 7 (b)

Table captions

Table 1: Comparison between experimental and theoretical magnetic moment (best fit of theoretical values shown).

Table 2: Classification of diffraction patterns obtained from the as-synthesized powders (15 particles analyzed per sample).

Table 3: Classifications of diffraction patterns obtained from lithium deficient material in the series $LiNi_{1-x}Mn_xO_2$ (x=0.3, 0.5,0.7) [15 particles of each analyzed].

Table 1

Starting material			
composition	**μ_{exp}**	**Model**	**μ_{theo}**
$Li_{1.02}Ni_{0.69}Mn_{0.29}O_2$	$3.54\mu_B$	$0.3Ni^{+2}$, $0.4Ni^{+3}$, $0.3Mn^{+4}$	$3.56\mu_B$
$Li_{0.99}Ni_{0.50}Mn_{0.52}O_2$	$3.11\mu_B$	$0.5Ni^{+2}$, $0.5Mn^{+4}$	$3.35\mu_B$
$Li_{1.02}Ni_{0.30}Mn_{0.70}O_2$	$3.06\mu_B$	$0.3Ni^{+2}$, $0.4Mn^{+3}$, $0.3Mn^{+4}$	$3.14\mu_B$
Delithiated material			
$Li_{0.88}Ni_{0.68}Mn_{0.29}O_2$	$2.50\mu_B$	$0.3Mn^{+4}$, $0.16Ni^{+2}$, $0.54Ni^{+3}$(LS) $0.3\ Mn_{+4}$, $0.26Ni^{+3}$(LS),$0.3Ni^{+2}$, Ni^{+4}(LS)	$2.55\mu_B$ $2.46\mu_B$
$Li_{0.86}Ni_{0.48}Mn_{0.53}O_2$	$3.05\mu_B$	$0.44Ni^{+2}$,$0.06Ni^{+4}$,$0.5Mn^{+4}$	$3.08\mu_B$
$Li_{0.87}Ni_{0.31}Mn_{0.65}O_2$	$3.03\mu_B$	$0.17Ni^{+2}$, $0.13Ni^{+3}$(LS), $0.4Mn^{+3}$(LS),$0.3Mn^{+4}$ $0.235Ni^{+2}$, $0.065Ni_{+4}$(LS), $0.3Mn^{+4}$, $0.4Mn^{+3}$(LS)	$2.99\mu_B$ $2.96\mu_B$

Table 2

Diffraction type	$LiNi_{0.7}Mn_{0.3}O_2$	$LiNi_{0.5}Mn_{0.5}O_2$	$LiNi_{0.3}Mn_{0.7}O_2$
O3	14 (93%)	3 (20%)	2 (13 %)
Spinel	1 (7%)	2 (13%)	3 (20%)
monoclinic		2 (13%)	
$\sqrt{3}a_{hex} \times \sqrt{3}a_{hex}$ R30^o		8 (54%)	10 (67%)

Table 3

Diffraction type	$Li_{0.88}Ni_{0.68}Mn_{0.29}O_2$	$Li_{0.86}Ni_{0.48}Mn_{0.53}O_2$	$Li_{0.87}Ni_{0.31}Mn_{0.65}O_2$
O3	8 (53%)	4 (27%)	3 (20%)
O3+extra reflection	-	1(6%)	-
Spinel	4 (27%)	3 (20%)	2 (13%)
Monoclinic	3 (20%)	2 (13%)	3 (20%)
$\sqrt{3}a_{hex}$ x $\sqrt{3}a_{hex}$ R30^o	-	5 (33%)	7 (47%)